Geochemistry, Geophysics, Geosystems
December 2008 ; Volume 9 (12) : Pages 1-13
http://dx.doi.org/10.1029/2007GC001845

An edited version of this paper was published by AGU.

Subseafloor stratigraphic profiling and soil classification from piezocone tests: A case study in the Gulf of Lion (NW Mediterranean Sea)

S. Lafuerza[1], J. Frigola[1], M. Canals[1,*], G. Jouet[2], M. Bassetti[3], N. Sultan[2] and S. Berné[2,3]

[1] GRC Geociències Marines, Departament d'Estratigrafia, Paleontologia i Geociències Marines, Universitat de Barcelona, Martí i Franquès s/n, 08028 Barcelona, Spain
[2] Institut Français de Recherche pour l'Exploitation de la Mer (IFREMER), BP 70, 29280 Plouzané, France
[3] Université de Perpignan IMAGES, 52 avenue Paul Alduy, Perpignan, France

*: Corresponding author : M. Canals, email address : miquelcanals@ub.edu

Abstract:

We show the results provided by piezocone tests in determining the stratigraphic profile and the soil classification of two drilling sites in the outer shelf and the upper slope of the Gulf of Lion, PRGL2 and PRGL1, respectively. Correlations with grain-size data indicate that sleeve friction can be used for profiling fine-grained sediments (site PRGL1), whereas cone tip resistance is the most adequate for sequences made of alternations of coarse- and fine-grained intervals (site PRGL2). Normalized cone resistance and friction ratio proved to be also appropriate for soil stratigraphy as it depicts trends in the coarse fraction of the tested soil. Silts and clays present in similar proportions at site PRGL1 responded to piezocone testing as pure clays usually do. Consequently, classical soil classification methods resulted in erroneous interpretation of these sediments as clays, whereas classification of the heterogeneous deposits at PRGL2 was consistent with the grain size. When tied to a high-resolution seismic reflection profile, the stratigraphy interpreted from the piezocone profile matches with the main seismic sequences and discontinuities defined from seismic stratigraphy analysis. Graded bedding also matches with cone tip resistance and sleeve friction data.

Keywords: piezocone; stratigraphy; soil classification; Gulf of Lion

1. Introduction

[2] The EC funded "Profiles Across Mediterranean Sedimentary Systems 1" (PROMESS 1) research project was designed to obtain very long sediment cores and perform in situ physical measurements from two continental margins in the Mediterranean Sea [Berné et al., 2004a]. In the Gulf of Lion, drilling and in situ testing were carried out at two sites: PRGL1 in the upper slope at 298 m of water depth (mwd) and PRGL2 in the outer shelf at 103 mwd (Figure 1). Five boreholes were drilled at site PRGL1 site (PRGL1_1 to PRGL1_5) and two at site PRGL2 (PRGL2_1 and PRL2_2). In this technical brief we compare the stratigraphic profile and soil type classification interpreted from piezocone measurements performed at sites PRGL1_3 and PRGL2_1 with grain size data acquired from sediment cores at PRGL1_4 and PRGL2_2 and with high-resolution seismic reflection profiles. The aim of this study is to illustrate the advantages of piezocone tests for (1) soil classification and stratigraphic profiling of marine sediments before drilling and (2) for the lithostratigraphic interpretation of seismic reflection profiles.

2. Materials and methods

Piezocone tests (CPTU) were performed using a down-hole cone penetration system that enable CPTU from the base of the borehole in sites PRGL1_3 and PRGL2_1, reaching penetration depths of 150 and 100 mbsf, respectively. The down-hole system latches into the lower end of a drill pipe by applying mud pressure in the borehole, while down-hole data are recorded. The system requires a drilling apparatus for advancing the borehole and a bottom hole assembly that permits latching the thrust machine, of 90 kN capacity. The maximum stroke of the thrust machine is 3 m. This system enables the borehole to be advanced and CPTUs be performed at every depth. Direct measurements of cone tip resistance (q_c), sleeve friction (f_s) and pore pressure (u_2) were recorded at a constant penetration rate of $2 cm \cdot s^{-1}$. CPTU were performed before drilling for coring providing a reliable lithostratigraphic profile.

Derived parameters from CPTU, such as the normalized cone resistance (Q_t), the friction ratio (FR) and the pore pressure ratio (B_q) (see Notations), allow the identification of the soil type using the soil classification charts proposed by Robertson (1990) and Ramsey (2002). Both methods define nine soil classes according to Q_t/FR and Q_t/B_q ratios but numbers are referred to soil classes distinctly (Figs. 2 and 3). Changes in profiles of q_c, f_s, have been followed for delineating the stratigraphic profile and the ratio of Q_t/FR for correlating with grain size curves. q_c and Q_t respond to variations in the resistance generated by the coarse fraction whereas f_s and FR illustrate changes in the cohesive fraction, which usually corresponds to the fine-grained fraction (Lunne et al., 1997).

The total sediment core recovery from PRGL1_4 and PRGL2_2 was 300 and 100 m, respectively. Grain-size analyses were carried out in both the bulk and the carbonate free fractions using a Laser Particle Sizer (LPS) Coulter LS100 at PRGL1_4 (Frigola et al., 2008 personal communication) and a LSP Coulter LS230 at PRGL2_2 (Bassetti et al., this issue). Since laser diffraction methods are claimed to underestimate plate-shaped clay mineral percentages, we consider the clay-silt limit at 8μm following the method proposed by Konert and Vandenberghe (1997). The particle sizes considered are: (i) clays with diameter (ϕ) between 0 and 8 μm; (ii) silts with $8<\phi<63$ μm and (iii) sands with $\phi > 63$ μm.

Geotechnical stratigraphy derived from CPTU was correlated with the seismic stratigraphy established by several authors. Six seismic sequences (S0 to S5), corresponding to 100 ky glacial-interglacial cycles, are bounded by major erosion surfaces (D30 to D70) (Berné et al., 2004a and this issue; Rabineau et al., 1998 and 2005). Within the last sequence (S5), other relevant secondary unconformities (D65, D64, D63 and D61) are identified (Jouet et al., 2006 and see review by Bassetti et al., this issue).

3. Results

3.1. CPTU tests at PRGL1 site

At PRGL1_3 the cone tip resistance, q_c, and the pore water pressure, u_2, increase quasi-linearly with depth, whereas the sleeve friction, f_s, depicts a more variable profile (Fig. 4). Note that the three-m-spaced negative peaks in u_2 curves are losses in CPTU readings, and therefore, are unrelated to soil type changes. Five geotechnical-stratigraphic units were identified based f_s values trend. These units have been numbered from I to V from top to bottom. Subunits are identified by alphabetical subindexes (Fig. 4). Soil classifications charts in Figures 2 and 3 predict that the geotechnical unit I consists of silty clays and clays whereas units from II to V are uniformly made by clays. Figure 4 shows the soil type based on the Q_t/FR chart from Robertson's (Fig. 2) at corresponding depths.

Correlation of Q_t/FR and grain-size profiles illustrates the correspondence between Q_t/FR and the silt/clay ratio (Fig. 5), supporting the sedimentological interpretation of the soil classes in Figures 2 and 3. Furthermore, unit boundaries (red dotted lines, Figs. 4 and 5) correspond to marked decreases in clay content accompanied by an evident increase in sand fraction, as observed by increases in Q_t/FR. The coincidence of these sharp changes with the end of CPTU sequences suggests those unit boundaries at 36 and 72 mbsf can be located within units IIb and IIId, respectively. In these levels and to a lesser extent at IVd, pronounced positive peaks in Q_t/FR correspond to sand content augmentations (Fig. 5). Main changes in the clay fraction, such as those in subunits IIb, IIId and IVd are clearly identified from the f_s profile (Fig. 6). The inverse variation between Q_t/FR and the clay fraction supports the clay-dependence of FR and f_s, as well as the silt dependence of Q_t. This, in addition, confirms the 8 μm size as an adequate clay-silt limit for laser grain-size measurements.

3.2. CPTU tests at PRGL2 site

In PRGL2, five geotechnical-stratigraphic units are identified based on changes in q_c (Fig. 7) and named 1 to 5 from top to bottom, and subdivided using alphabetically ordered subindexes. q_c and f_s curves are highly similar, with relative high values for sands (from 0 to 28.6 mbsf and from 67 to the borehole bottom) and relative low values in clays (from 28.6 to 68 mbsf and from 78.3 to 82.3 mbsf) (Fig. 8). Zero u_2 values through the upper 30 meters and negative values at the borehole bottom are attributed to readings in sands affected by cavitation processes (Lunne et al., 1997). Soil types based on the Q_t/FR chart from Robertson classification at corresponding depths are also shown in Figure 7. The good correlation between the sand content profile and Q_t/FR profile supports geotechnical stratigraphy for site PRGL2. Geotechnical units have been correlated with the lithological units defined for this site by Bassetti et al. (this issue) and we found good correlation. However, we grouped them in five major units for ease of consistency

with resistance values whereas the lithological profile identified 14 units (Bassetti et al., this issue). At the borehole bottom (99.24-100.13 mbsf), these authors identify a very coarse clastic unit that we have included in geotechnical subunit 5c.

The soil types interpreted from CPTU classifications (Figs. 2 and 3) are highly consistent with the grain size distribution (Fig. 8). Graded-bedding is identified from q_c at intervals where the sampling resolution from grain size analysis is insufficient to detect them. This is illustrated by the overall coarsening-upwards trend of subunit 1d and the interval comprised by subunits 5b and 5c, and the fining-upwards trend of subunits 4a, 4b and 4c and by subunit 5a. Changes of the fine fraction content, which is made of clayey silts, are well depicted by the $1/Q_t$ profile.

4. Discussion

4.1. Soil classification from CPTU measurements

Correlations of grain-size curves with CPTU sediment type classifications at site PRGL1 indicate that the percentage of silts and clays ranges between 40 and 60% along the borehole (Fig. 4). Units II to V are made of a mixture of silts and clays instead of mainly clays, as suggested by CPTU classifications (Figs. 2 and 3). This can be attributed to similar (undrained) piezocone penetration of silts and clays when they occur in similar proportions. In contrast, piezocone testing in sediments with heterogeneous grain-size, where drainage conditions occur (Lunne et al., 1997), as in PRGL2, allows accurate sediment type attribution (Fig. 7). On the other hand, in deposits where mixtures of cohesionless (silty sands to gravels) sediments are present, as in PRGL2, soil changes are better detected from cone tip resistance, q_c, as it responds more precisely to changes in drainage conditions than sleeve friction, f_s (Fig. 7).

We have found a good correlation between Robertson's (1990) and Ramsey's (2002) soil classification methods. However, when cavitation occurs, as in PRGL2, the Q_t/FR ratio should be used in isolation for soil-type interpretation. Gravelly sands and sands may induce temporary cavitation adjacent to the pore-water pressure sensor location, making the Q_t/Bq model unreliable (Ramsey, 2002). For correlating with grain size we, therefore, have used only Robertson's (1990) classification based on Q_t/FR (Figs. 4 and 7), although the one from Ramsey (2002) can be also considered since both classifications identify the same soil types (Figs. 2 and 3).

Water pressures generate significant values of cone resistance and pore pressure, which are corrected to zero at seafloor. In down-hole CPTU systems, the pressure conditions in the drill pipe may not be in full equilibrium with the surrounding ground water pressure. Consequently, zero-correction can be subject to increased uncertainty that is in the order of 100 kPa (Peuchen,

2000). The uncertainty for the zero-correction of the cone tip resistance is approximately equivalent to a factor representing the net area ratio effect, which is 0.75 for the data presented herein. The zero drift of the measured q_c and u_2 is considered to be within the allowable minimum accuracy according the accuracy class selected by Fugro, following standardized practice (ISSMGE, 1999). Therefore, we consider irrelevant the uncertainty of the derived parameters used for soil classification.

4.2. Stratigraphic profiling from CPTU profiles

The transition from one layer to another is not necessarily registered as a sharp change in cone tip resistance, q_c (Lunne et al., 1997). Recent numerical analyses show that q_c in a dense sandy layer embedded in soft clays is less than its true value when the thickness of the sand layer is less than 28 cone diameters (Ahmadi and Robertson, 2005), i.e. >1 m for the cone used in our study. In contrast, for a very loose sand layer under moderate stress states (effective vertical stress ≥ 70 kPa) the layer should be more than eight cone diameters, i.e. >0.3 m for our study. The lower thickness of sand layers identified at PRGL2, which is 1.5 m in subunit 1c (Fig. 7), is slightly above the 0.3-1 m cone accuracy.

Some authors (Robertson, 1990, Lunne et al., 1997) consider that the sleeve friction, f_s, is less accurate than the cone tip resistance q_c and that the pore pressure u_2 measurements since f_s measures average values over the sleeve length (13 cm in our case), which tends to smooth out the record of thin layers. However, we found f_s to be the most accurate CPTU parameter for profiling the sediments at PRGL1 site, as demonstrated by its correlation with the clay content (Fig. 6). The stratigraphic profile based on f_s is further supported by the Q_t/FR profile, which proves that f_s variations are, at this site, caused by changes in the cohesion that are directly related to the clay content.

4.3. Correlation between CPTU based geotechnical stratigraphy and high resolution seismic reflection profiles

At site PRGL2, lithological and geotechnical subunits 1a to 1d correspond to the upper shoreface sands of the seismic unit U152 (Fig. 9a, Bassetti et al., this issue). Our sandy Unit 1 is bounded by a submarine erosion surface D65 atop of the geotechnical Unit 2. Subunits 2a and 2b, separated by discontinuity D64, display clays with intercalations of silty clays of a lower shoreface and correspond to the seismic unit U151 (Fig. 10a). The top of the silty clayey subunit 2c, which is characterized by a slight increase in q_c and f_s, corresponds to combined discontinuity D60-D63, which separates seismic sequence S5 (formed here by U152 and U151) from S4. D63 is an erosion surface attributed to a drop of sea-level during the overall sea-level fall between Marine Isotope Stage (MIS) 3 and MIS 2 (Jouet et al., 2006, Bassetti et al., this

issue). Clays in our subunits 2d and 2e correspond to the distal part of seismic sequence S4. The sandy Unit 3 corresponds to foreshore-upper shore shoreface deposits that, in conjunction with the clayey subunit 4a forms seismic unit S3. The underlying fining upwards subunit 4b constitute seismic unit S2. The top of Unit 3 corresponds to seismic discontinuity D50 and the base of subunit 4b corresponds to the combined surfaces D45-D40-D35. Subunit 5a is separated of the coarsening upwards subunits 5b and 5c by discontinuity D30, which is at the base of seismic sequence S0.

At the much more lithologically homogeneous site PRGL1, we found a likely correspondence amongst units I to III and IV with seismic sequences S5 and S4, respectively (Fig. 10b). Subunits IIb (from 33 to 36 mbsf), IIId (70-72 mbsf) and IVd (120-127 mbsf) comprise the reflectors corresponding to discontinuities D63, D60 and D50, which are found to represent intervals of variable thickness characterized by low friction measurements due to increased sand content (Figs. 5 and 6). The lower Unit V corresponds to S3. The rest of the boundaries between our CPTU based subunits do correspond to specific seismic reflectors, which are seen to separate different seismic facies: subunits IIa and IIIc correspond to low amplitude hemi-stratified facies; IIIb, IVa, IVb, Va and Vb to facies of intermediate amplitude; and IIIa, IIIb and IVc to facies of higher relative amplitude. Such changes in relative amplitude in the seismic record do correlate well with the CPTU based geotechnical-stratigraphic divisions.

5. Conclusions

The piezocone (CPTU) is a widely accepted soil classification test routinely used by geotechnical engineers. However, CPTU soil classification charts have to be used with extreme care when dealing with mixtures of marine silts and clays in similar proportions. The (undrained) behavior of these admixtures is the same as (undrained) pure clays and, consequently, they could be erroneously classified as clays. Combined normalized tip resistance Q_t and friction ratio FR profiles are very useful to identify grain-size trends in these sediment types and verify soil type classification results.

The comparison of CPTU profiles with grain-size data and high resolution seismic reflection profiles has demonstrated that amongst the various CPTU parameters, sleeve friction is convenient for profiling fine-grained sediments, such as those found at PRGL1 site, whereas cone tip resistance proves to be the best suited parameter in heterogeneous sequences with coarse and fine-grained sediments as at PRGL2 site. The ratio of the normalized tip resistance vs friction ratio Q_t/FR has proved to be also suitable for identifying soil stratigraphy.

From the case study presented herein we conclude that in situ piezocone tests are a useful tool to interpolate and extrapolate the stratigraphic profile and the soil classification on the basis of grain-size and/or seismic reflection data. The drawbacks found in the prediction of fine-grained deposits illustrate the need to further investigate soil classification methods in these sediment types.

Acknowledgements

The authors thank the EC PROMESS1 project (contract num. EVR1-CT-2002-40024). The onboard scientific party of the project has been involved in the gathering of the data and their input is very much appreciated. We thank G. Herrera (Universitat de Barcelona) for grain size analyses and E. Thereau (Ifremer) for processing the seismic data. We also acknowledge all other researchers and technicians from PROMESS1 partner institutions that have contributed in different ways to this research. Associate Editor as well as G. Verdiccio and an anonymous reviewer are thanked for their review of the manuscript. S. Lafuerza benefits from a PhD research grant by the Spanish Ministry for Education and Science. GRC Geociències Marines is funded by Generalitat de Catalunya research grants program to high quality scientific groups (ref. 2005 SGR-00152).

References

Ahmadi, M.M. and P.K. Robertson (2005), Thin-layer effects on the CPT q_c measurements. *Can. Geotech. J., 42,* 1302-1317.

Bassetti, M.A., Berné, S., Jouet, G., Taviani, M., Dennielou, B., Flores, J.A., Gaillot, A., Gelfort, R., Lafuerza, S. and Sultan, N., (this issue), 100-kyr and rapid sea-level changes recorded by prograding shelf sand bodies in the Gulf of Lions (Western Mediterranean Sea).

Berné, S., M. Rabineau, J.A. Flores and F.J. Sierro (2004a), The Impact of Quaternary global changes on strata formation, exploration of the shelf edge in the northwest Mediterranean Sea, *Oceanography, 17* (4), 92-117.

Berné, S., Carré, D., Loubrieu, B., Mazé, JP., Morvan, L., Normand, A. (2004b), Le Golfe du Lion, *Carte morpho-bathymétrique 1/250000*. Edition Ifremer, isbn 2-84433-140-8.

Berné, S., Jouet, G. and the Promess 1 science party (this issue), Sedimentary sequences and sea-level changes during the last 500 kyrs. The Gulf of Lions revisited by the Promess 1 drilling operation.

Canals, M. (1985), Estructura sedimentaria y evolución morfológica del talud y el glacis continentales del Golfo de León: Fenómenos de desestabilización de la cobertura cuaternaria, PhD thesis, University of Barcelona, 618 pp.

ISSMGE (1999), International reference test procedure for the Cone Penetration Test (CPT) and the Cone Penetration Test with Pore Pressure (CPTU), report of the ISSMGE Technical Committee 16 on Ground Property Characterisation from in-situ testings, Proceedings of the Twelfth European conference on Soil mechanics and geotechnical Engineering, Amsterdam, ed. Barends et al., 3, 2195-2222.

Jouet, G., S. Berné, M. Rabineau, M.A. Bassetti, P. Bernier, B. Dennielou, J.A. Flores, F.J. Sierro and M. Taviani (2006), Shoreface migrations at the shelf edge and sea-level changes around the last glacial maximum (Gulf of Lions, NW Mediterranean), *Mar. Geol., 234*, 21-42.

Konert, M. and J. Vandenberghe (1997), Comparison of laser grain size analysis with pipette and sieve analysis: a solution for the underestimation of the clay fraction. *Sedimentology, 44*, 523-535.

Lunne, T., P.K. Robertson J.J.M. Powell (1997), *Cone Penetration Testing in geotechnical practice*, 312 pp, Blackie academic/EF Spon, Rutledge Publishing Company, New York.

Medimap Group (2005), Morpho-bathymetry of the Mediterranean Sea. CIESM/IFREMER special publication, Atlases and Maps, two maps at 1/2 000 000.

Peuchen, J. (2000), Deepwater Cone Penetration Tests, OTC 12094, Offshore technology Conference, Houston, Texas, 1-4 May 9 pp.

Rabineau, M., S. Berné, E. Ledrezen, G. Lericolais, T. Marsset and M. Rotuno (1998), 3D architecture of lowstand Quaternary sand bodies on the outer shelf of the Gulf of Lions, France, *Mar Petrol Geol*, *15* (5), 439-452.

Rabineau, M., S. Berné, D. Aslanian, J.-L. Olivet, P. Joseph, F. Guillocheau, J.F. Bourillet, E. Ledrezen and D. Granjeon (2005), Sedimentary sequences in the Gulf of Lion: A record of 100,000 years climatic cycles, *Mar Petrol Geol*, *22*, 775-804.

Ramsey, N. (2002), A calibrated model for the interpretation of cone penetration tests (CPTs) in North Sea Quaternary soils, paper presented at the Offshore site investigation and geotechnics: diversity and sustainability, London, 26-28 November.

Robertson, P. K. (1990), Soil classification using the cone penetration test. *Can Geotech J*, *27*, 151-158.

Figure captions

Figure 1. Location of the PRGL2 (42º50'58.20''N, 003º39'3085''E) and PRGL1 (42º41'23.30''N, 003º50'15.50''E) sites. CCC, Cap de Creus Canyon; LDC, Lacaze-Duthiers Canyon; PC, Pruvot Canyon; AC, Aude Canyon; HC, Hérault Canyon; SC, Sète Canyon; MC, Montpellier Canyon; PRC, Petit Rhône Canyon; GRC, Grand Rhône Canyon. Bathymetry in meters from Berné et al. (2004b) and Medimap Group (2005). 100 m contour equidistance unless otherwise indicated. Names after Canals (1985).

Figure 2. Soil type classifications for PRGL1 and PRGL2 sites plotted on Robertson's (1990) charts for normalized parameters Q_t, FR and Bq.

Figure 3. Soil type classifications for PRGL1 and PRGL2 sites plotted on Ramsey's (2002) charts for normalized parameters Q_t, FR and Bq.

Figure 4. CPTU profiles from PRGL1_3 borehole. Red dotted lines are unit boundaries that correspond to main seismic discontinuities. Blue dotted lines indicate subunit boundaries. Robertson's (1990) soil types based on Q_t/FR are represented at corresponding depths. Numbers in the soil type scale correspond to those in Figure 2.

Figure 5. Correlation between the profile of the ratio Q_t/FR and grain-size distribution profiles from PRGL1. Grain-size analyses were performed at 1:80 cm resolution. Sand contents correspond to both the bulk fraction (BF) and the carbonate free fraction (CFF).

Figure 6. Correlation between the sleeve friction f_s profile and the clay content from PRGL1.

Figure 7. CPTU profiles from PRGL2_1 borehole. Red dotted lines are unit boundaries that correspond to main seismic discontinuities. Blue dotted lines indicate subunit boundaries. Soil types are based on the Q_t/FR chart from Robertson's (1990). Numbers in the soil type scale correspond to those in Figure 2.

Figure 8. Correlation between profiles of the ratio Q_t/FR and $1/Q_t$ and grain-size distribution profiles from PRGL2. Grain-size analyses were performed at 1:20 cm resolution in muddy sections and at 1:80 cm in cohesionless sandy sections.

Figure 9. Grain size trends at PRGL2 interpreted from cone tip resistance q_c trends. A: coarsening-upwards sequence at subunit 1d; B: fining-upwards sequence at unit 7; C: fining-

upwards sequence at subunits 4c, 4b and 4a; and D: coarsening-upwards sequence at subunits 5c and 5b.

Figure 10. Correlation between CPTU based geotechnical stratigraphy and seismic reflection stratigraphy at PRGL1 and PRGL2 sites. A: CPTU-seismic reflection data correlation at site PRGL2 and B: CPTU-seismic reflection data correlation at site PRGL1.

Notations

Symbol	**Description, units**
q_c	cone tip resistance, kPa
f_s	sleeve friction, kPa
u_2	pore pressure, kPa
q_t	corrected cone resistance, equal to $q_c + u_2(1\text{-}a)$, kPa
q_{net}	net tip resistance, equal to $q_{net} = q_t - \sigma v$, kPa
a	cone area ratio (0.75 in this study)
σv	total vertical stress relative to seafloor
Q_t	normalized cone resistance, equal to $Q_t = (q_t - \sigma v) / \sigma' v$, dimensionless
$\sigma' v$	vertical effective stress, kPa
FR	friction ratio, equal to $f_s / q_c \cdot 100$, %
B_q	pore pressure ratio, equal to $\Delta u/q_{net}$, dimensionless
Δu	in situ excess pore pressure, equal to $u_2 - u_0$, kPa
u_0	in situ pore pressure, equal to $\gamma_w \cdot z$ (γ_w, water unit weight; z, depth), kPa
ϕ	particle diameter, μm

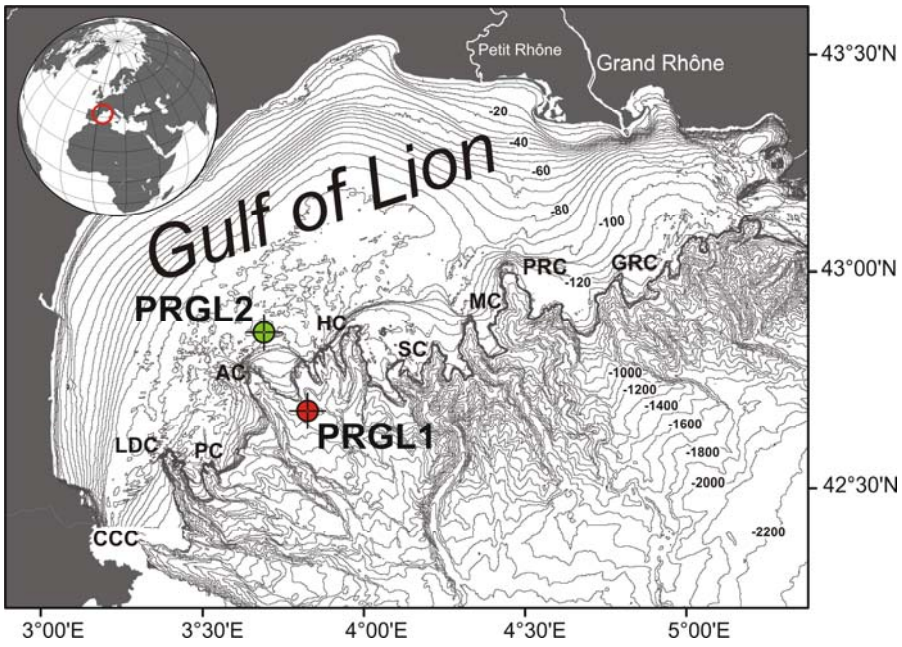
Petit Rhône
Grand Rhône
Gulf of Lion
PRGL2
PRGL1
HC
SC
AC
MC
PRC
GRC
LDC
PC
CCC
-20
-40
-60
-80
-100
-120
-1000
-1200
-1400
-1600
-1800
-2000
-2200
43°30'N
43°00'N
42°30'N
3°00'E
3°30'E
4°00'E
4°30'E
5°00'E

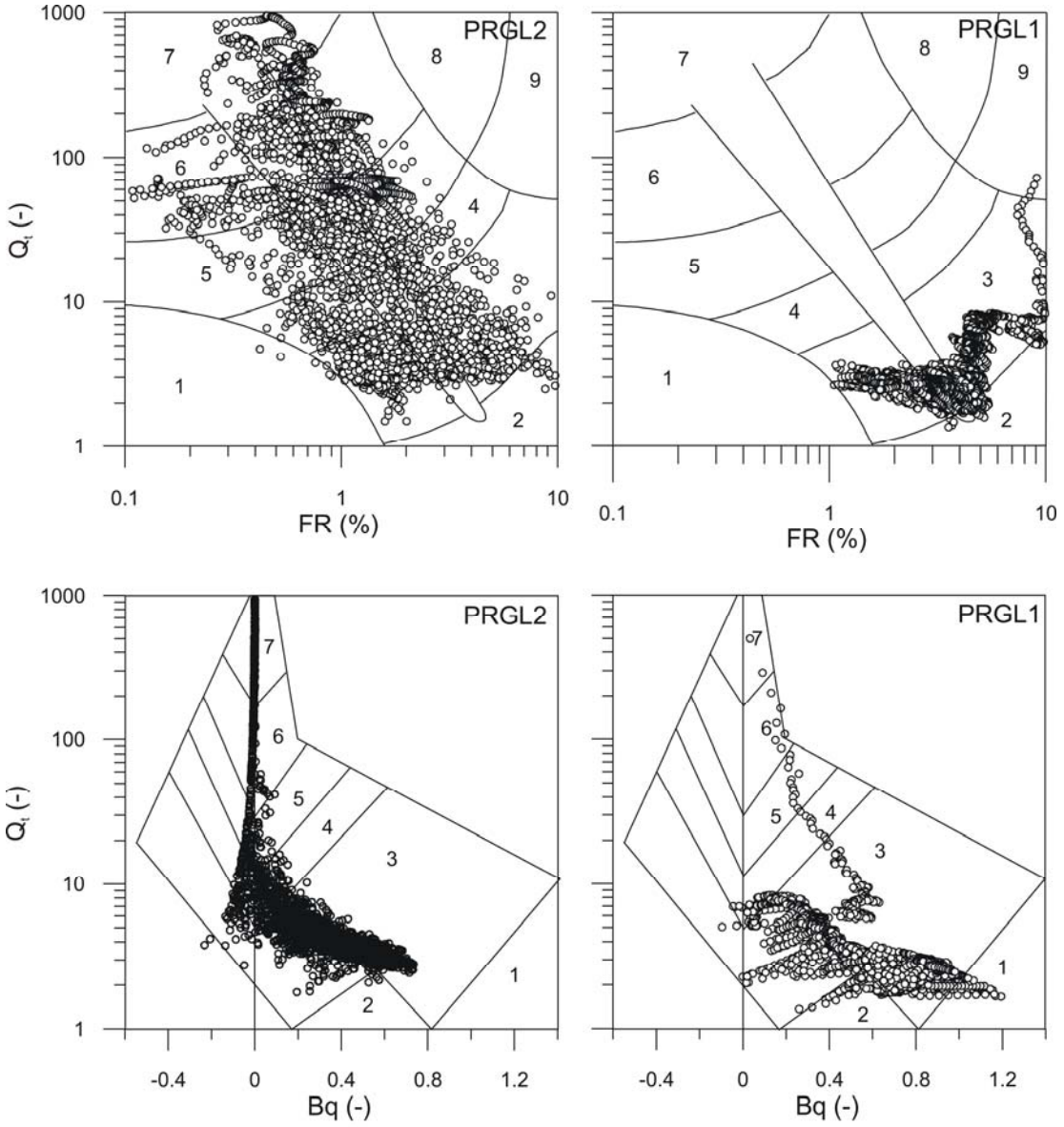

Soil types from Robertson (1990):

1 - Sensitive fine grained; 2 - Organic soils-peats; 3 - Clays; 4 - Silt mixtures clayey silt to silty clay; 5 - Sand mixtures, silty sand to sand silty; 6 - Sands; clean sands to silty sands; 7 - Gravelly sand to sand; 8 - Very stiff sand to clayey sand; 9 - Very stiff fine grained.

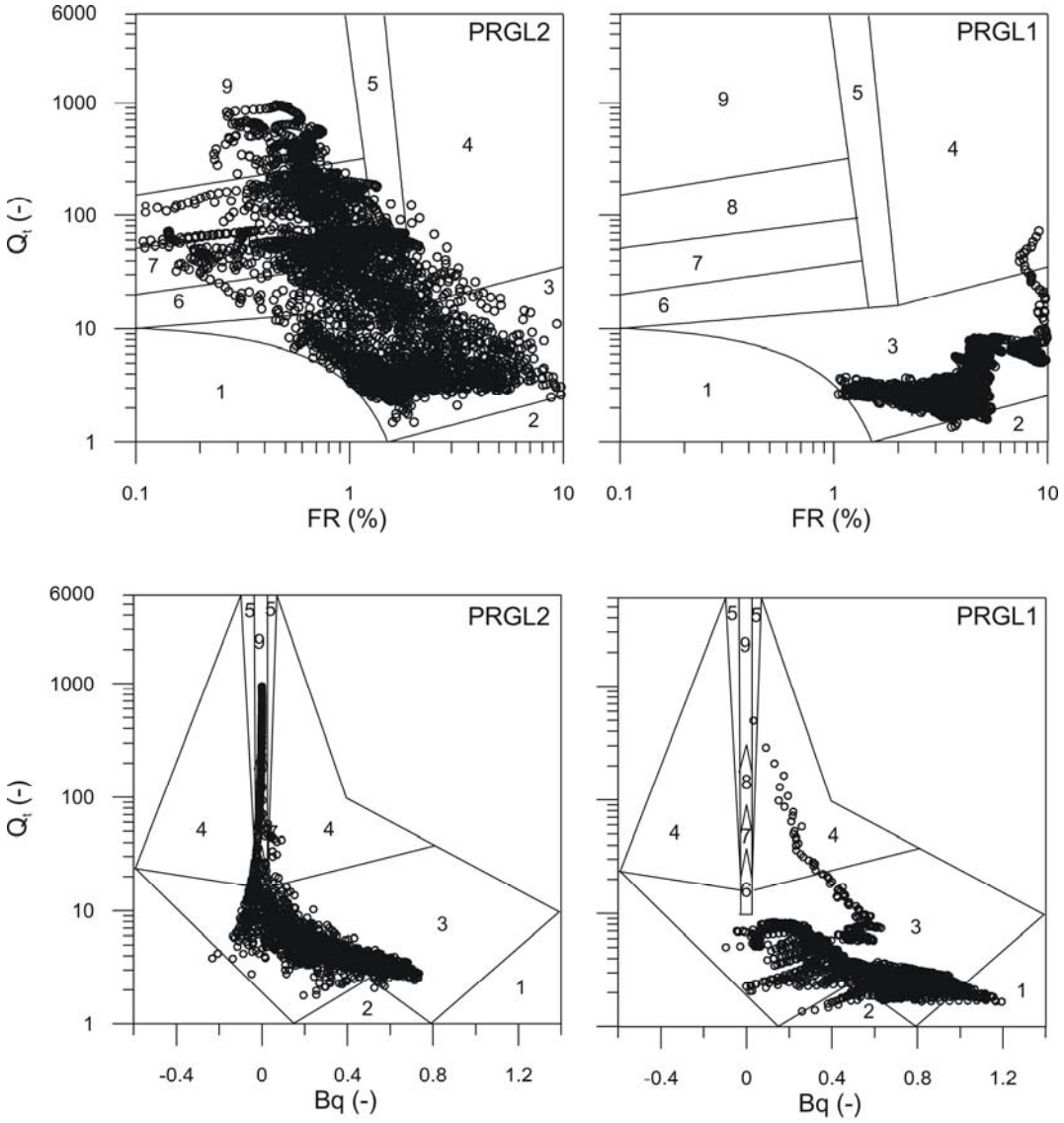

Soil types from Ramsey (2002):

1 - Extra sensitive clay; 2 - Organic clay and peat; 3 - Clay (S_u/p'_0<1); 4 - Clay (S_u/p'_0>1); 5 - Clayey sand; 6 - Sandy very clayey silt; 7 - Sandy silt; 8 - Silty sand; 9 - Clean sand.

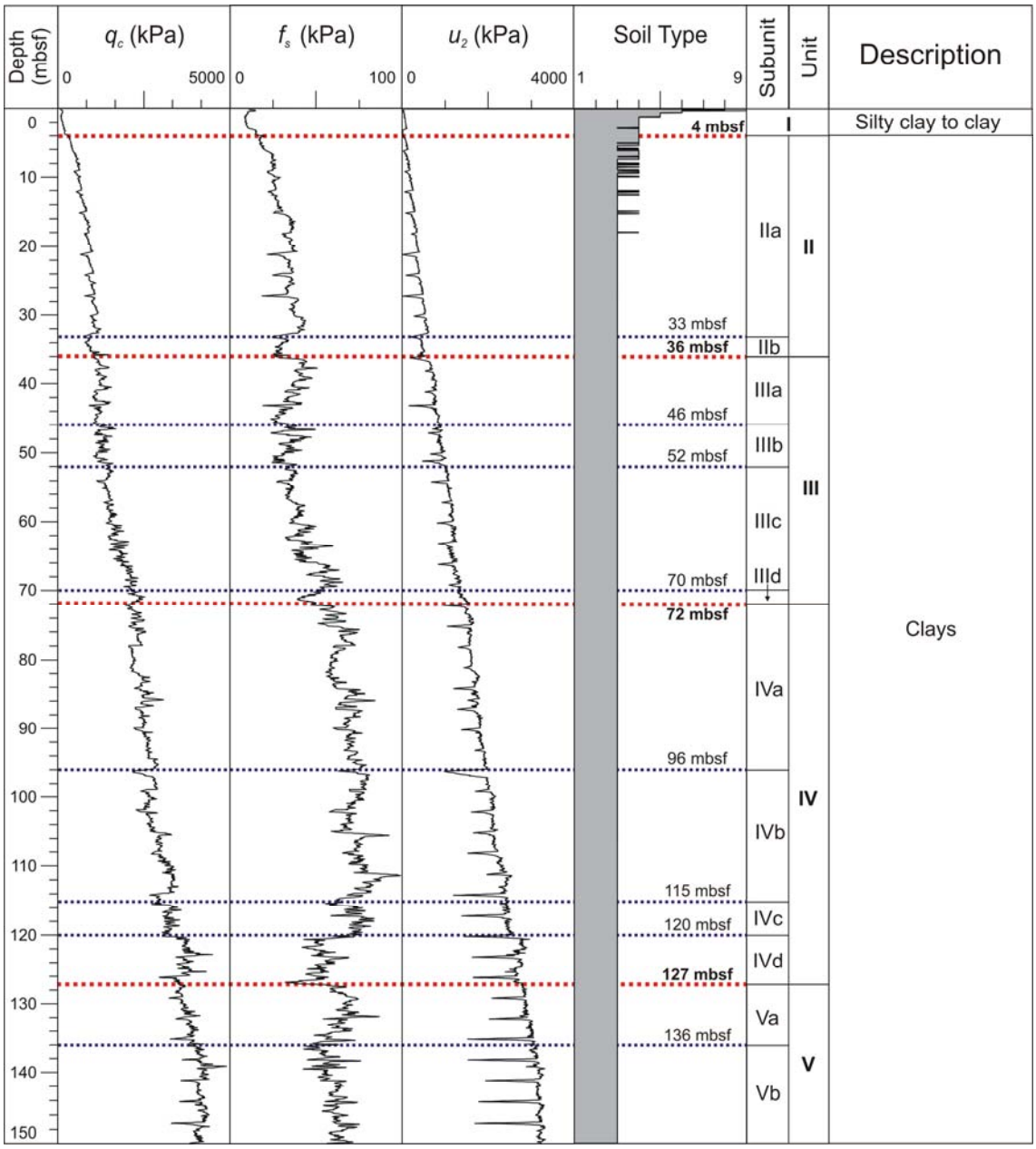
Depth (mbsf)
q_c (kPa)
0
5000
f_s (kPa)
0
100
u_2 (kPa)
0
4000
Soil Type
1
9
Subunit
Unit
Description
0
10
20
30
40
50
60
70
80
90
100
110
120
130
140
150
4 mbsf
33 mbsf
36 mbsf
46 mbsf
52 mbsf
70 mbsf
72 mbsf
96 mbsf
115 mbsf
120 mbsf
127 mbsf
136 mbsf
I
IIa
IIb
IIIa
IIIb
IIIc
IIId
IVa
IVb
IVc
IVd
Va
Vb
II
III
IV
V
Silty clay to clay
Clays

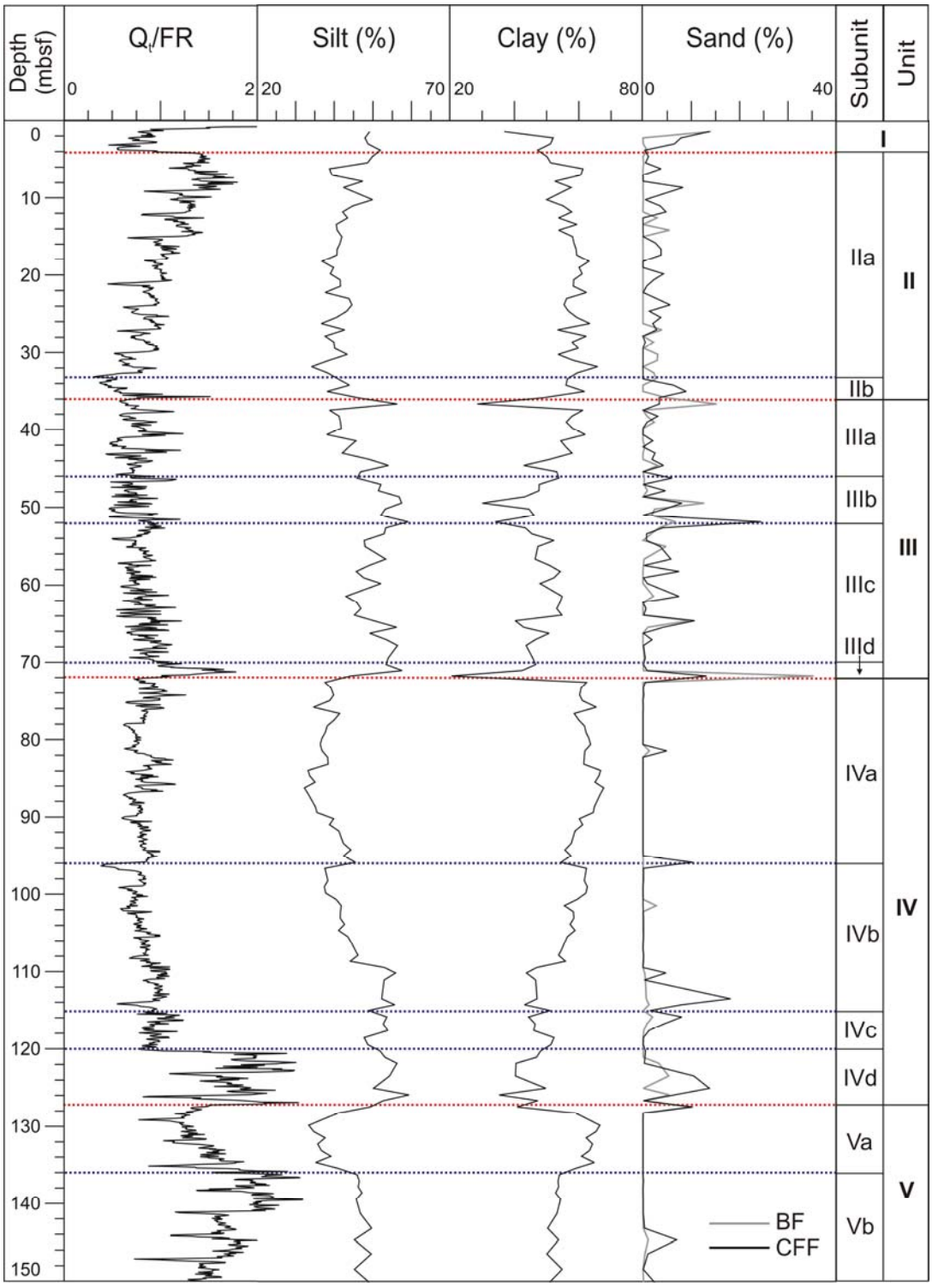
Depth (mbsf)
Q$_t$/FR
0
2
Silt (%)
20
70
Clay (%)
20
80
Sand (%)
0
40
Subunit
Unit
0
10
20
30
40
50
60
70
80
90
100
110
120
130
140
150
I
IIa
IIb
IIIa
IIIb
IIIc
IIId
IVa
IVb
IVc
IVd
Va
Vb
II
III
IV
V
BF
CFF

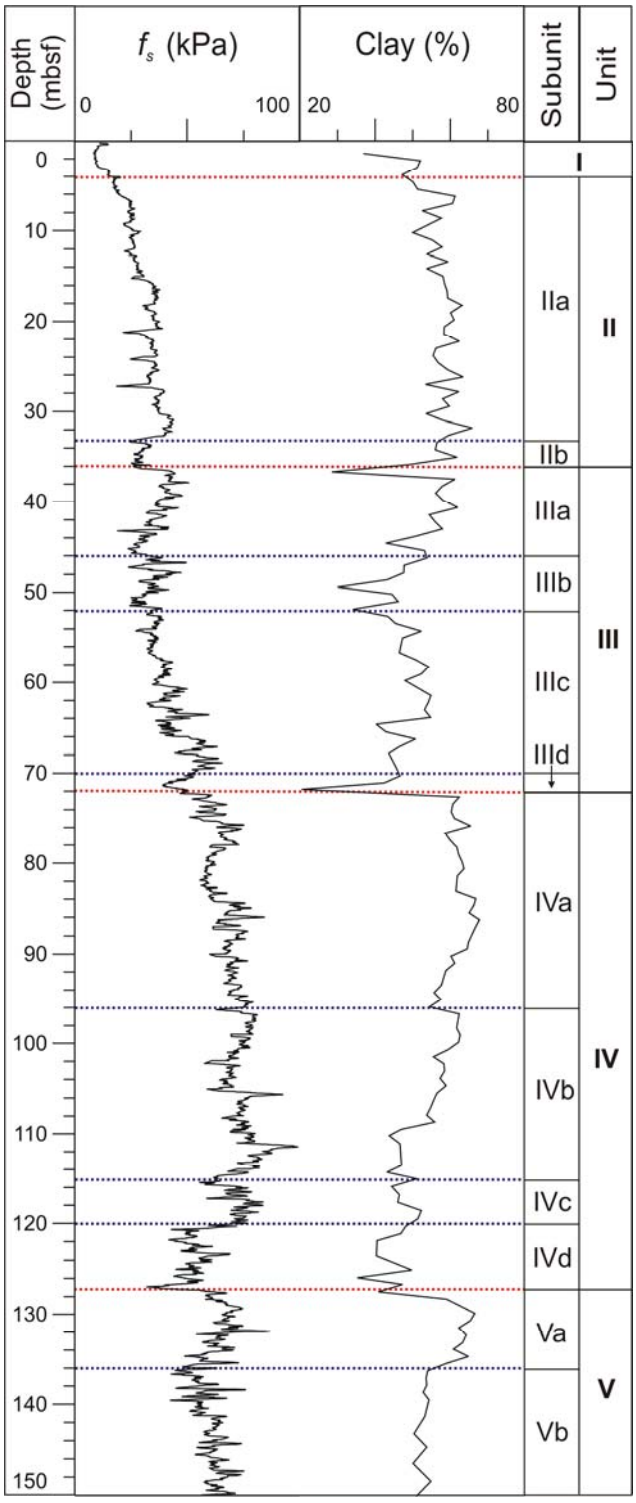
Depth (mbsf)
f_s (kPa)
0
100
Clay (%)
20
80
Subunit
Unit
0
10
20
30
40
50
60
70
80
90
100
110
120
130
140
150
I
IIa
IIb
II
IIIa
IIIb
IIIc
IIId
III
IVa
IVb
IVc
IVd
IV
Va
Vb
V

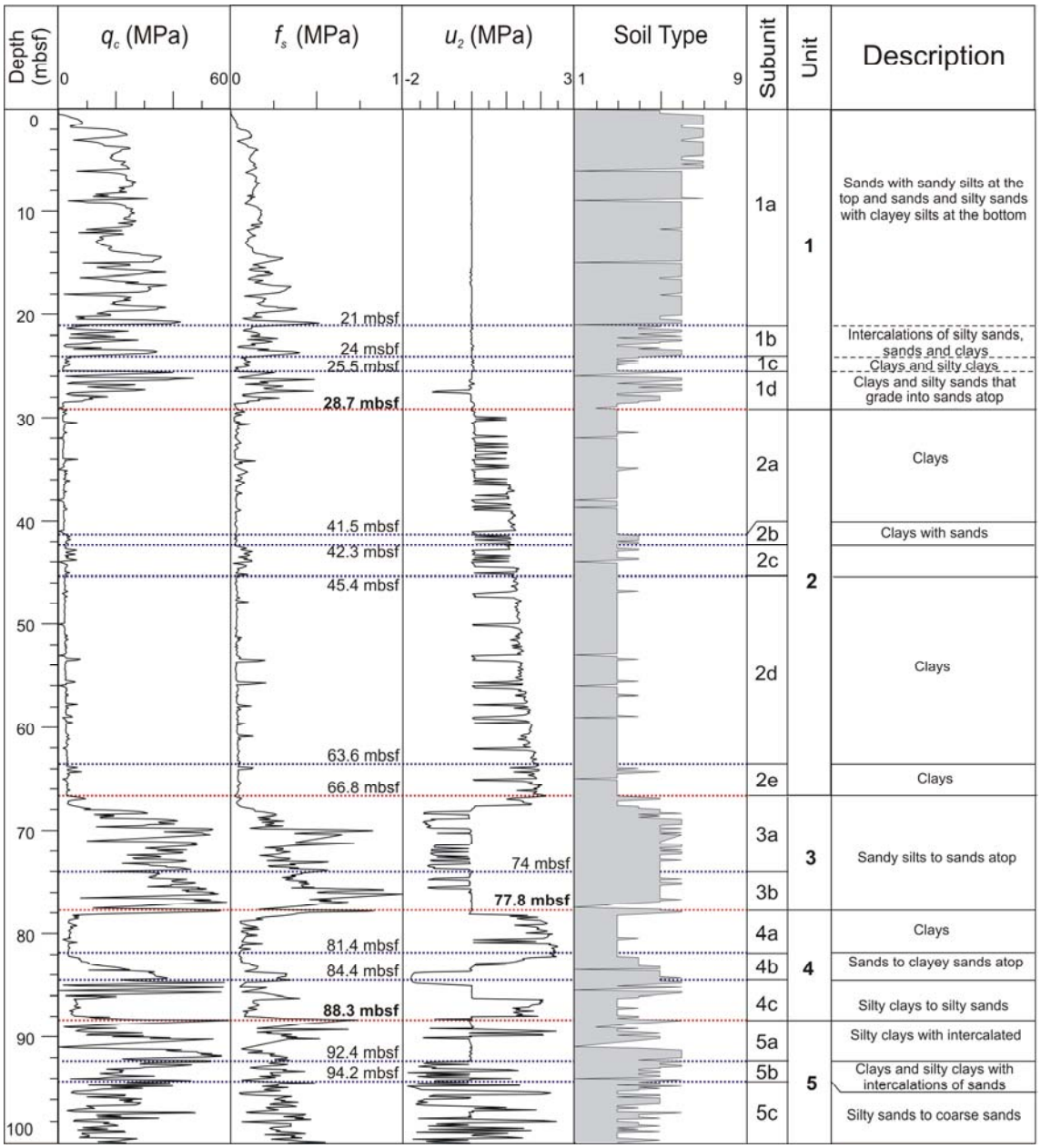
Depth (mbsf)
q_c (MPa)
0
60
f_s (MPa)
0
1
u_2 (MPa)
-2
3
Soil Type
1
9
Subunit
Unit
Description
0
10
20
30
40
50
60
70
80
90
100
21 mbsf
24 msbf
25.5 mbsf
28.7 mbsf
41.5 mbsf
42.3 mbsf
45.4 mbsf
63.6 mbsf
66.8 mbsf
74 mbsf
77.8 mbsf
81.4 mbsf
84.4 mbsf
88.3 mbsf
92.4 mbsf
94.2 mbsf
1a
1b
1c
1d
2a
2b
2c
2d
2e
3a
3b
4a
4b
4c
5a
5b
5c
1
2
3
4
5
Sands with sandy silts at the top and sands and silty sands with clayey silts at the bottom
Intercalations of silty sands, sands and clays
Clays and silty clays
Clays and silty sands that grade into sands atop
Clays
Clays with sands
Clays
Clays
Sandy silts to sands atop
Clays
Sands to clayey sands atop
Silty clays to silty sands
Silty clays with intercalated
Clays and silty clays with intercalations of sands
Silty sands to coarse sands

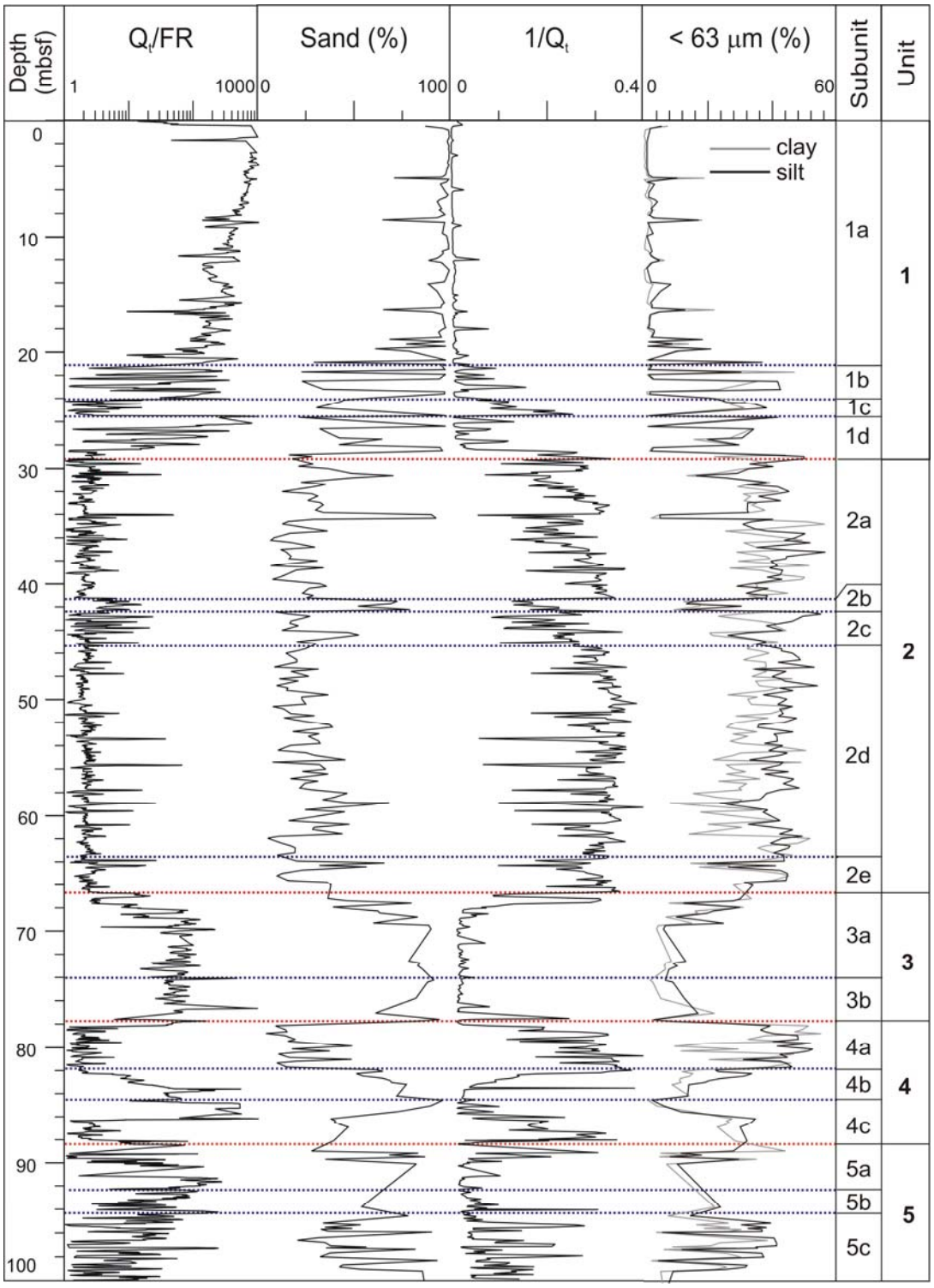
Depth (mbsf)
Qt/FR
1
1000
Sand (%)
0
100
1/Qt
0
0.4
< 63 μm (%)
0
60
Subunit
Unit
clay
silt
0
10
20
30
40
50
60
70
80
90
100
1a
1b
1c
1d
2a
2b
2c
2d
2e
3a
3b
4a
4b
4c
5a
5b
5c
1
2
3
4
5

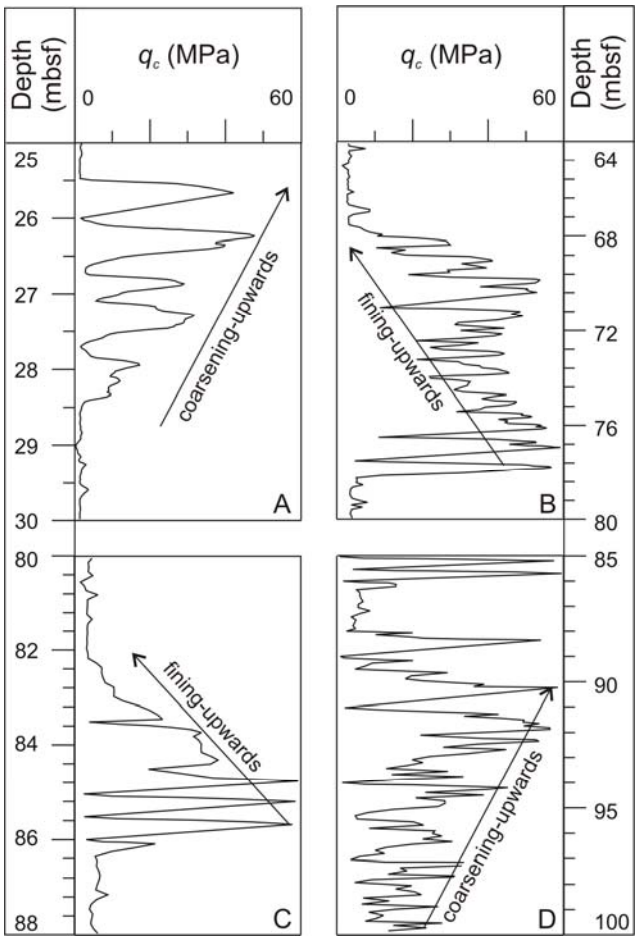
Depth (mbsf)
q_c (MPa)
0
60
25
26
27
28
29
30
coarsening-upwards
A
q_c (MPa)
0
60
Depth (mbsf)
64
68
72
76
80
fining-upwards
B
80
82
84
86
88
fining-upwards
C
85
90
95
100
coarsening-upwards
D

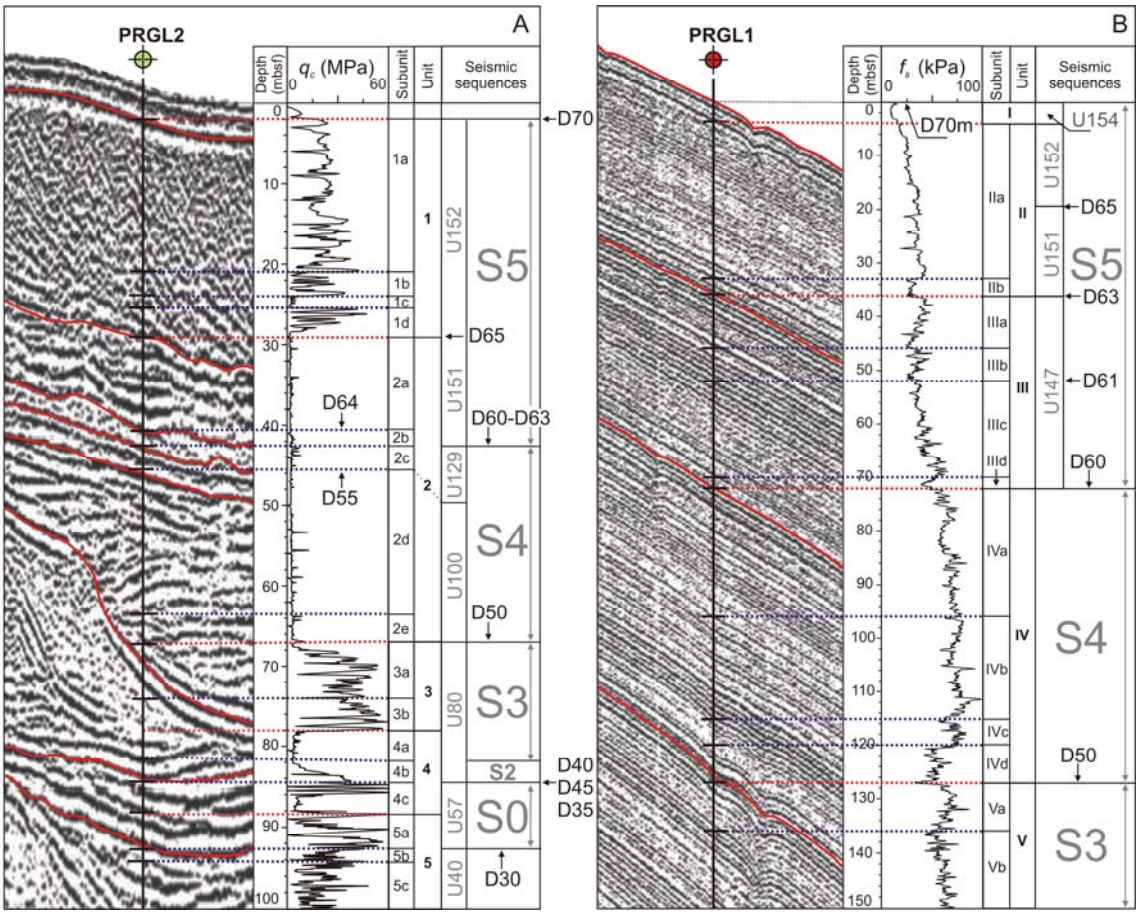
A
PRGL2
Depth (mbsf)
q_c (MPa)
0
60
Subunit
Unit
Seismic sequences
D70
D65
D64
D60-D63
D55
D50
D40
D45
D35
D30
1a
1b
1c
1d
2a
2b
2c
2d
2e
3a
3b
4a
4b
4c
5a
5b
5c
1
2
3
4
5
U152
U151
U129
U100
U80
U57
U40
S5
S4
S3
S2
S0
B
PRGL1
f_s (kPa)
0
100
D70m
U154
D65
D63
D61
D60
D50
I
II
III
IV
V
IIa
IIb
IIIa
IIIb
IIIc
IIId
IVa
IVb
IVc
IVd
Va
Vb
U147